THE JOURNAL OF BIOLOGICAL CHEMISTRY VOL. 287, NO. 33, pp. 28152–28162, August 10, 2012

Mutant p53 Aggregates into Prion-like Amyloid Oligomers and Fibrils

IMPLICATIONS FOR CANCER[*] [S]

Received for publication, January 7, 2012, and in revised form, June 9, 2012 Published, JBC Papers in Press, June 19, 2012, DOI 10.1074/jbc.M112.340638

Ana P. D. Ano Bom[‡§1], Luciana P. Rangel[‡§1], Danielly C. F. Costa[‡§], Guilherme A. P. de Oliveira[‡§], Daniel Sanches[‡§], Carolina A. Braga[‡§], Lisandra M. Gava[§¶], Carlos H. I. Ramos[§‖], Ana O. T. Cepeda[¶], Ana C. Stumbo[**], Claudia V. De Moura Gallo[§‡‡], Yraima Cordeiro[§ §§], and Jerson L. Silva[‡§2]

From the [‡]Instituto de Bioquímica Médica, [§]Instituto Nacional de Ciência e Tecnologia de Biologia Estrutural e Bioimagem, and [§§]Faculdade de Farmácia, Universidade Federal do Rio de Janeiro, Rio de Janeiro, RJ 21941-902, Brazil, the [‖]Instituto de Química and [¶]Instituto de Biologia, Universidade Estadual de Campinas, Instituto de Biologia, 13084-862 Campinas, SP, Brazil, the [‡‡]Departamento de Genética, IBRAG and [**]Departamento de Histologia e Embriologia, IBRAG, Universidade do Estado do Rio de Janeiro, RJ 20550-013 Rio de Janeiro, Brazil

Background: p53 function is lost in more than 50% of tumors.
Results: p53 aggregates into amyloid oligomers and fibrils *in vitro* and in breast cancer tissues; mutant p53 seeds amyloid aggregation of WT p53, a behavior typical of a prion.
Conclusion: Prion-like aggregation is crucial for the negative dominance of mutant p53.
Significance: The inhibition of aggregation could be a target for cancer therapy.

Over 50% of all human cancers lose p53 function. To evaluate the role of aggregation in cancer, we asked whether wild-type (WT) p53 and the hot-spot mutant R248Q could aggregate as amyloids under physiological conditions and whether the mutant could seed aggregation of the wild-type form. The central domains (p53C) of both constructs aggregated into a mixture of oligomers and fibrils. R248Q had a greater tendency to aggregate than WT p53. Full-length p53 aggregated into amyloid-like species that bound thioflavin T. The amyloid nature of the aggregates was demonstrated using x-ray diffraction, electron microscopy, FTIR, dynamic light scattering, cell viabilility assay, and anti-amyloid immunoassay. The x-ray diffraction pattern of the fibrillar aggregates was consistent with the typical conformation of cross β-sheet amyloid fibers with reflexions of 4.7 Å and 10 Å. A seed of R248Q p53C amyloid oligomers and fibrils accelerated the aggregation of WT p53C, a behavior typical of a prion. The R248Q mutant co-localized with amyloid-like species in a breast cancer sample, which further supported its prion-like effect. A tumor cell line containing mutant p53 also revealed massive aggregation of p53 in the nucleus. We conclude that aggregation of p53 into a mixture of oligomers and fibrils sequestrates the native protein into an inactive conformation that is typical of a prionoid. This prion-like behavior of oncogenic p53 mutants provides an explanation for the negative dominance effect and may serve as a potential target for cancer therapy.

Cancer is a leading cause of death worldwide. According to the World Health Organization (WHO), deaths from cancer will reach 11 million annually by 2030. Biomedical research has provided a great deal of information about cancer, but the molecular mechanisms that lead to cancer remain poorly understood. The role of the tumor suppressor protein p53 is regarded as vital, as p53 is a nuclear phosphoprotein that induces cell cycle arrest and apoptosis in response to cellular stress, particularly DNA damage. Moreover, mutations in the p53 gene (*TP53*) are strongly associated with increased susceptibility to cancer (1).

p53 is a tetrameric flexible protein containing 393 residues. The N-terminal activation domain is able to interact with a number of proteins, whereas the C-terminal domain is responsible for tetramerization. The central region or core domain (p53C) of the protein constitutes the sequence-specific DNA-binding region (2) and is the segment most involved in mutant-related tumors.

Previously, we showed that the core domain of p53 forms β-sheet-rich fibrillar aggregates under mild denaturing conditions (hydrostatic pressure) (3, 4). At that time, our group hypothesized that p53 aggregation could lead to cancer (3). In support of this view, it has been reported that p53 regions other than the DNA-binding domain may undergo aggregation under physiological conditions (5, 6). In addition, the largely unstructured N-terminal transactivation domain aggregates into fibrils when incubated at low pH (7). We found that small cognate DNAs stabilize the core domain and full-length p53 and have the potential to rescue aggregated, misfolded species (8). Recently, we demonstrated that mutant p53 co-localizes with amyloid-like protein aggregates in cancer biopsies (9). Finally, aggregated mutant p53 induces co-aggregation of wild-type p53 and its paralogs p63 and p73 (10). Therefore, the hypothesis that p53 aggregation may participate in some cancers similarly

* This work was supported by grants from Conselho Nacional de Desenvolvimento Científico e Tecnológico (CNPq), the Instituto Nacional de Ciência e Tecnologia de Biologia Estrutural e Bioimagem (INBEB), and the Fundação de Amparo à Pesquisa do Estado do Rio de Janeiro (FAPERJ) of Brazil.
⌘ *Author's Choice*—Final version full access.
[S] This article contains supplemental Table S1 and Figs. S1 and S2.
[1] Both authors contributed equally to this work.
[2] To whom correspondence should be addressed: Universidade Federal do Rio de Janeiro, Instituto de Bioquímica Médica, Bloco E Sala 10, Cidade Universitária, 21941–590, Rio de Janeiro, RJ, Brazil. Tel.: 55-21-25626756; Fax: 55-21-38814155; E-mail: jerson@bioqmed.ufrj.br.

to the situation in Alzheimer and Parkinson disease (11, 12) has attracted increasing attention (3, 4, 10).

Although p53 aggregation has been shown to occur (3–10, 13), we know little about the molecular mechanisms involved and its potential relevance to the tumorigenic process (14). The most frequent p53 mutation found in cancers is the hot-spot mutation R248Q, which renders the protein unable to bind cognate DNA and exert its proper functions (15, 16). Here, we asked whether wild-type p53 and R248Q could form aggregates under physiological conditions, what the properties of these aggregates would be and whether mutant p53 aggregates could seed aggregation of the wild-type isoform. The morphology, structure, kinetics, and toxicity of the aggregates were characterized at pH 7.2 and 5.0 for the first time using electron microscopy, dot-blots, x-ray diffraction, FTIR, and LIVE/DEAD viability assays. We found that full-length p53 undergoes amyloid aggregation in a pattern similar to that of the p53 core domain. In addition, we performed immunofluorescence co-localization assays and found positive amyloid aggregation in a tumor sample bearing the R248Q mutant and in breast cancer tumoral cell lines. This result corroborates our *in vitro* finding that R248Q has a higher propensity to aggregate than wild-type p53. Most interestingly, a mixture of amyloid oligomers and fibrils of R248Q were found to seed the aggregation of wild-type p53 in a prion-like fashion. This prion-like aggregation behavior would explain the negative dominance of mutant p53, and this knowledge may help in developing new therapeutic strategies to prevent or control cancer progression.

EXPERIMENTAL PROCEDURES

Chemicals—All reagents were of analytical grade. Distilled water was filtered and deionized through a Millipore water purification system.

Subcloning, Expression, and Purification of WT p53C and R248Q—p53C (comprising amino acid residues 94 to 312) subcloning, expression, and purification were performed as previously described (3).

p53C Aggregation—Three aggregation procedures were employed using 5 μM of p53C, as follows. The HT aggregate procedure consisted of subjecting proteins to increasing temperatures, varying from 25 to 60 °C, at 5 °C increments and allowing the proteins to remain at each temperature for 10 min. The 37T aggregate procedure consisted of incubating p53C at 37 °C for 2 h. The HP aggregate procedure consisted of pressure-induced aggregation performed at 37 °C, in which proteins were submitted to increasing pressures up to 3 kbar in ~500-bar increments, and the samples were incubated for 8 min at each pressure. The pressure cell was purchased from ISS (Champaign, IL). All measurements were performed using 50 mM Tris, pH 7.2 or 70 mM sodium acetate pH 5.0 as buffers, and both buffers contained 150 mM NaCl, 5 mM DTT, and 5% (v/v) glycerol.

Circular Dichroism (CD) Measurements—CD experiments were carried out using a Jasco J-715 spectropolarimeter (Jasco Corporation, Japan) and a 0.01-cm path length quartz cuvette. Far-UV spectra of 25 μM for WT or R248Q p53C were monitored from 200 to 260 nm and averaged over 3 scans. The buffer (50 mM Tris pH 7.2 or 70 mM sodium acetate pH 5.0, both containing 150 mM NaCl, 5 mM DTT, and 5% (v/v) glycerol) baselines were subtracted from their respective sample spectra.

Thioflavin T Fluorescence—Thioflavin T (ThT)[3] fluorescence was acquired using an ISS-PC1 spectrofluorimeter (ISS, Champaign, IL) with excitation at 450 nm and emitted light collected in the 470 to 530 nm range. p53C (5 μM) was incubated with 50 μM ThT, and the temperature or pressure was increased to obtain the HT or HP aggregates, respectively. To measure the aggregation kinetics, soluble p53C (5 μM) was incubated at 37 °C for 2 h (37T aggregate) with 25 μM ThT. ThT emission was collected over time at 480 nm (the excitation was set at 450 nm). p53 samples were routinely centrifuged at 14,000 rpm/15 min prior to the experiments to eliminate any background aggregation signal.

Dynamic Light Scattering (DLS)—DLS data of soluble oligomeric species (obtained after centrifugation of p53C aggregates at 14,000 rpm/15min) were acquired using a DynaPro NanoStar instrument (Wyatt Technology) with three independent acquisitions of 10 measurements each.

Fourier Transformed Infrared (FTIR) Spectroscopy—After aggregation, the samples were dialyzed against water and further lyophilized and were then deposited directly on the ATR surface of a Nicolet 6700 IR instrument (Thermo Corp.). The amide I region (1700–1600 cm^{-1}) was deconvoluted using OMNIC software (Thermo Corp.), and the secondary structure components were assigned as previously described (17, 18).

Transmission Electron Microscopy (TEM)—The ultrastructure of the p53C aggregates (HT aggregate, 37T aggregate and HP aggregate) was analyzed using TEM in a Jeol 1200 EM operated at 80 kV using negative staining. Samples were adhered to a carbon-coated grid and stained with a 2% solution of uranyl acetate prepared in water.

Dot-blot Assay—Aggregates of WT p53C and mutant R248Q at pH 7.2 or 5.0 were placed onto a nitrocellulose membrane at a concentration of 50 μM in a final volume of 10 μl. The membrane was blocked with TBS-T (10 mM Tris-HCl, 0.15 M NaCl pH 8.0, 0.1% Tween 20) + 5% nonfat milk for 2 h at room temperature and incubated for 18 h at 4 °C with the primary antibody A11 (which recognizes several types of amyloid oligomers (19)) at a 1:1,000 dilution (Chemicon, CA). The membrane was then washed with TBS-T and incubated with an HRP-conjugated secondary antibody at a 1:10,000 dilution for 1 h at room temperature in TBS-T + 5% nonfat milk. After five washes with TBS, the membrane was developed using an ECL kit (GE Healthcare, Buckinghamshire, UK). We used bovine serum albumin (BSA) and soluble WT p53C as negative controls. The aggregate of the amyloidogenic protein TTR (transthyretin) was used as a positive control.

X-ray Fibril Diffraction—x-ray diffraction of fibrils was measured using the D03B-MX1 beamline at the National Laboratory of Synchrotron Light (Campinas, SP, Brazil). The wavelength used was $\lambda = 1.488$ Å, the distance between the sample and the CCD detector (MarResearch) was 100 mm, and the

[3] The abbreviations used are: ThT, thioflavin T; DLS, dynamic light scattering; FTIR, Fourier transformed infrared; TEM, transmission electron microscopy; PrP, prion protein; SEC, size-exclusion chromatography; TTR, transthyretin.

image was acquired at a fixed angle for 15 min and recorded using AutoMar software (MarResearch).

Cytotoxicity Assay—Vero cells were maintained in DMEM-high glucose supplemented with 10% fetal bovine serum at 37 °C in a 5% CO_2 atmosphere. After reaching 80% confluence, cells were plated in 24-well plates, and the aggregates were added at a 4 μM final concentration. After 48 h, the cells were tested with the LIVE/DEAD Viability/Cytotoxicity Assay kit (Invitrogen). Cell fluorescence was visualized under an LSM 510 meta fluorescence microscope (Carl Zeiss International, Oberkochen, Germany). The buffers used included the following: 10 mM Tris and 10 mM NaCl, pH 7.2; or 10 mM MES and 10 mM NaCl, pH 5.0.

Congo Red Binding to Aggregates and Birefringence Analysis—Evaluation of Congo red binding to p53 aggregates was carried out according to Lai *et al.* (20). Briefly, after protein aggregation in CRBB (Congo red binding buffer), containing 5 mM phosphate, 150 mM KCl, pH 7.5, 1 μM p53C samples were incubated with Congo red (Sigma) at 10 μM. After 30 min, the absorbance of the suspension at 477 and 540 nm was measured, and the amount of Congo red bound to amyloid fibrils (mol of Congo red bound/liter of suspension) was calculated with the following formula: $A_{540\ nm}/25{,}295\text{-}A_{477\ nm}/46{,}306$. For polarization microscopy (21), these aggregates were washed three times with CRBB and the ressuspended pellets were transferred to glass slides and cover slides. p53C aggregates stained with Congo red were analyzed using a Olympus BX51 light microscope equipped with polarizers.

Immunofluorescence Co-localization Assay in Archived Breast Cancer Biopsies—Paraffin-embedded tumor biopsies from five breast cancer cases diagnosed as invasive ductal carcinoma and previously analyzed for TP53 mutational status were obtained from the Department of Pathology at the Fernandes Figueira Institute (IFF-FIOCRUZ) in Rio de Janeiro, Brazil. Briefly, tumor sections were incubated in 10 mM citrate buffer at pH 6.0 and 55 °C for 20 min for antigen retrieval, and nonspecific antigenic sites were blocked with PBS/BSA 5%. Next, sections were labeled with the A11 primary antibody (1:2,000) and then incubated with a donkey anti-rabbit Alexa Fluor 555-conjugated secondary antibody. Next, these labeled sections were incubated with a mouse monoclonal anti-human p53 protein DO-1 primary antibody (1:200), which was followed by incubation with a donkey anti-mouse Alexa Fluor 488-conjugated secondary antibody. In both cases, the primary antibodies were incubated overnight at 4 °C, and the secondary antibodies were incubated for 1 h at room temperature in a moist and dark chamber. The samples were washed and mounted and analyzed under a confocal laser scanning microscope (LSM 510 META, Carl Zeiss Inc.). The study was approved by the local research ethics committee.

Cell Culture of Tumoral Cell Lines—The human breast carcinoma cell lines MCF-7 (wild-type p53) and MDA-MB 231 (mutated p53 - p.R280K.) were obtained from the American Type Culture Collection (ATCC, Manassas, VA). MCF-7 cells were cultured in DMEM containing 1.0 g/liter glucose supplemented with 2.0 g/liter HEPES, 3.7 g/liter sodium bicarbonate, 10% fetal bovine serum, and 5 μg/ml bovine insulin. MDA-MB 231 cells were cultured in DMEM containing 4.5 g/liter glucose supplemented with 2.0 g/liter HEPES, 3.7 g/liter sodium bicarbonate, and 10% fetal bovine serum. A total of 100 units/ml penicillin and 100 μg/ml streptomycin were added to the culture plates prior to the experiments. The cells were maintained at 37 °C in a humidified atmosphere containing 5% CO_2.

Size-exclusion Chromatography (SEC) and Western Blotting Analysis of the Fractions—To analyze the degree of p53 aggregation in cell lines, we have lysed both MCF-7 (WT) and MDA-MB-231 (R280K) cells in a buffer containing Tris-HCl 5 mM, NaCl 150 mM, 0.5% sodium deoxycholate, and protease inhibitor mixture (Sigma) using liquid nitrogen. The lysate was centrifuged for 5 min at 3,000 rpm and 250 μl of the supernatant was immediately loaded onto a Superdex S200 HR10/30 column (GE Healthcare) equilibrated in a buffer containing 50 mM Tris-HCl, 150 mM NaCl, 5 mM dithiothreitol, 5% glycerol, pH 7.5) using a 0.4 ml/min flow in a Shimadzu Ultra Fast Liquid Chromatograph. The eluted fractions were precipitated with trichloroacetic acid and washed with acetone. Cell extract fractions were resolved by SDS-PAGE (10%) and the separated proteins transferred to polyvinylidene difluoride (PVDF) membranes. The membranes were blocked overnight at 4 °C in Tris-buffered saline containing 1% Tween 20 (TBS-T) and 5% nonfat milk and incubated for 2 h with the primary antibody anti-p53 (DO-1) (1:10,000). Next, the membranes were washed with TBS-T and incubated with a peroxidase-conjugated secondary antibody (1:5,000) for 1 h. Immunoreactive bands were visualized by ECL Western blotting Detection System (GE Healthcare, Buckinghamshire, UK), according to the manufacturer's instructions.

Immunofluorescence Co-localization Assays in Breast Cancer Cell Cultures—The human breast epithelial carcinoma cell lines MCF-7 and MDA-MB 231 were washed twice with PBS (phosphate-buffered saline), fixed with formaldehyde solution (3.7%) and permeabilized with Triton X-100 (0.5%). The cells were then incubated with 5 mM ammonium chloride for 30 min, and nonspecific antigenic sites were blocked with PBS/BSA 3% (phosphate saline buffer/bovine serum albumin) for 2 h. The cells were simultaneously labeled with a mouse monoclonal anti-human p53 protein DO-1 primary antibody (1:200) and an anti-oligomer A11 primary antibody (1:1,000) for 2 h at room temperature. Next, the cells were incubated with anti-mouse Texas Red 561 and anti-rabbit IRDye® 680LT-conjugated secondary antibodies for 1 h at room temperature in a dark chamber. The cells were washed and analyzed using confocal laser scanning microscopy (LSM 510 Meta, Carl Zeiss Inc.).

RESULTS

Aggregation of Full-length p53 and p53C under Different Conditions—Previous studies have reported the buildup of p53 in tumor cells (9, 10, 22, 23), and we previously demonstrated the ability of p53C to form aggregates *in vitro* (3). To evaluate the mechanism of p53C aggregation in different environments, we initially characterized the aggregation kinetics of the wild-type and R248Q mutant forms of p53C at 37 °C and pH 7.2 or 5.0 (37T aggregate, Fig. 1). The aggregation into amyloid structures was monitored by measuring the binding of the protein to thioflavin T (ThT) (Fig. 1*A*), as ThT is known to bind both amyloid oligomers and fibrillar aggregates. Our results show

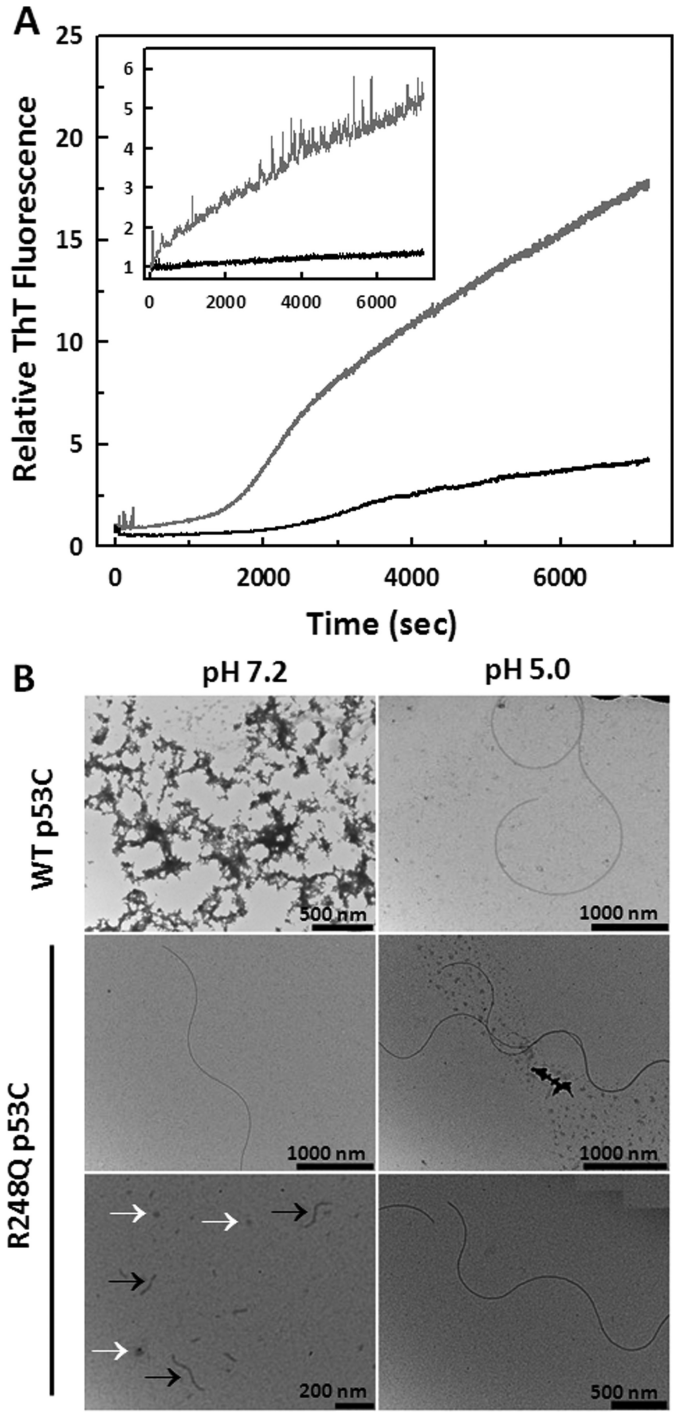

FIGURE 1. **Aggregation kinetics and morphology of WT p53C and mutant R248Q 37T aggregates.** *A*, samples at 5 μM were incubated at 37 °C for 2 h in the presence of ThT at a 5 ThT:1 protein molar ratio at pH 7.2 or pH 5.0. The aggregation was monitored over time based on the increase in ThT fluorescence emission (excitation 450 nm; emission 480 nm) for WT p53C at pH 7.2 (*black line*) and R248Q at pH 7.2 (*gray line*). *Inset*: WT p53C at pH 5.0 (*black line*) and R248Q at pH 5.0 (*gray line*). *B*, images obtained using 5 μM of each sample incubated at 37 °C for 30 min. *Black* and *white arrows* indicate fibrillar and oligomeric aggregates, respectively. Scale bars are shown in each figure.

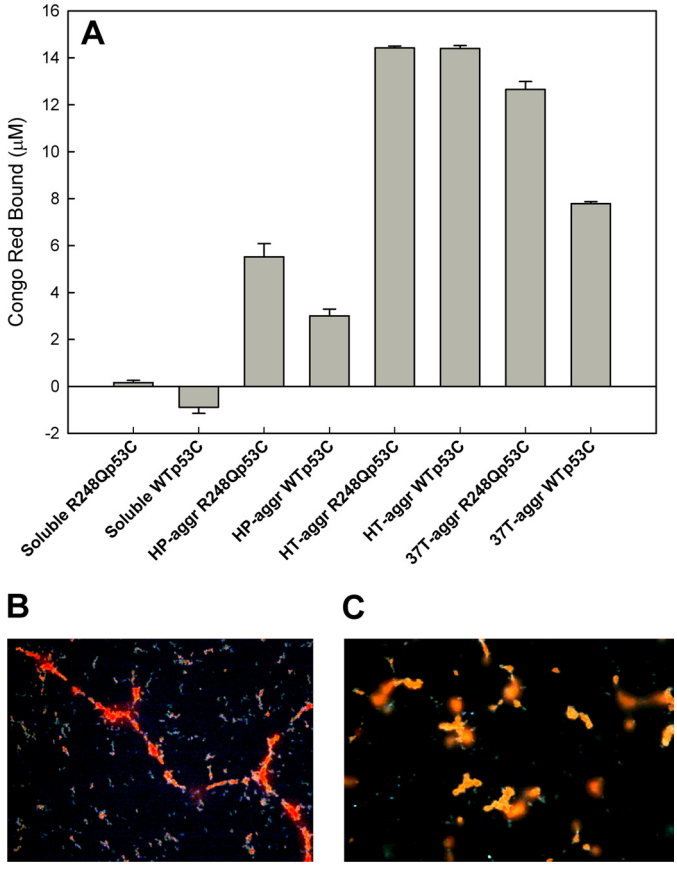

FIGURE 2. **Evaluation of amyloid nature of p53 aggregates by Congo red binding and birefringence.** *A*, soluble and aggregated WT and R248Q p53C samples at 1 μM (pH 7.2) were incubated with Congo Red at 1:10 molar ratio for 30 min. The extent of Congo Red binding to the 37T-aggregates is shown as μmol of bound Congo Red per liter of aggregate solution determined as described under "Experimental Procedures." *B* and *C*, Congo Red green birefringence visualized by polarized light microscopy of WT p53C HT-aggregate (*B*) and R248Q p53C HT-aggregate (*C*). The images were obtained at 400× magnification.

that p53C is prone to form aggregates when incubated for 2 h at 37 °C (37T aggregate). The R248Q mutant aggregates to a larger extent than wild-type p53C when incubated at pH 7.2. Accordingly, there was higher Congo red binding of aggregated R248Q p53C than aggregated WT p53C at pH 7.2 (Fig. 2*A*). In addition, Congo red birefringence analysis evidenced the amyloid character of WT p53C and R248Q p53C aggregates (Fig. 2, *B* and *C*). However, both proteins aggregated less at pH 5.0 (Fig. 1, *inset*). The studies at low pH were prompted by our previous findings that p53 (mutant and wild-type) proteins form molten globules at pH 5.0 (24) and the fact that acidic pH has been related to tumor environments (25).

To verify that the species generated in solution were typical amyloid forms, we examined their morphology using TEM. Fibrillar, oligomeric, and amorphous aggregates were observed in the electron micrographs of aggregates obtained under various conditions (Fig. 1*B*, *arrows*). Moreover, the heterogeneous aggregation of p53 resembled the aggregation of mammalian prion proteins (PrP) (26). We also analyzed the size distribution of 37T aggregates formed by p53C WT and R248Q using DLS. We were not able to determine the size of the high molecular weight aggregates observed at pH 7.2 due to the detection range of the equipment (from 0.1 to 1,000 nm). However, following centrifugation of the aggregates, the soluble oligomeric species could be characterized at both pH values, yielding a hydrodynamic radius (Rh) of 66 ± 4 nm (% polydispersity = 3.1) for the R248Q mutant at pH 5.0. Even after centrifugation, the oligo-

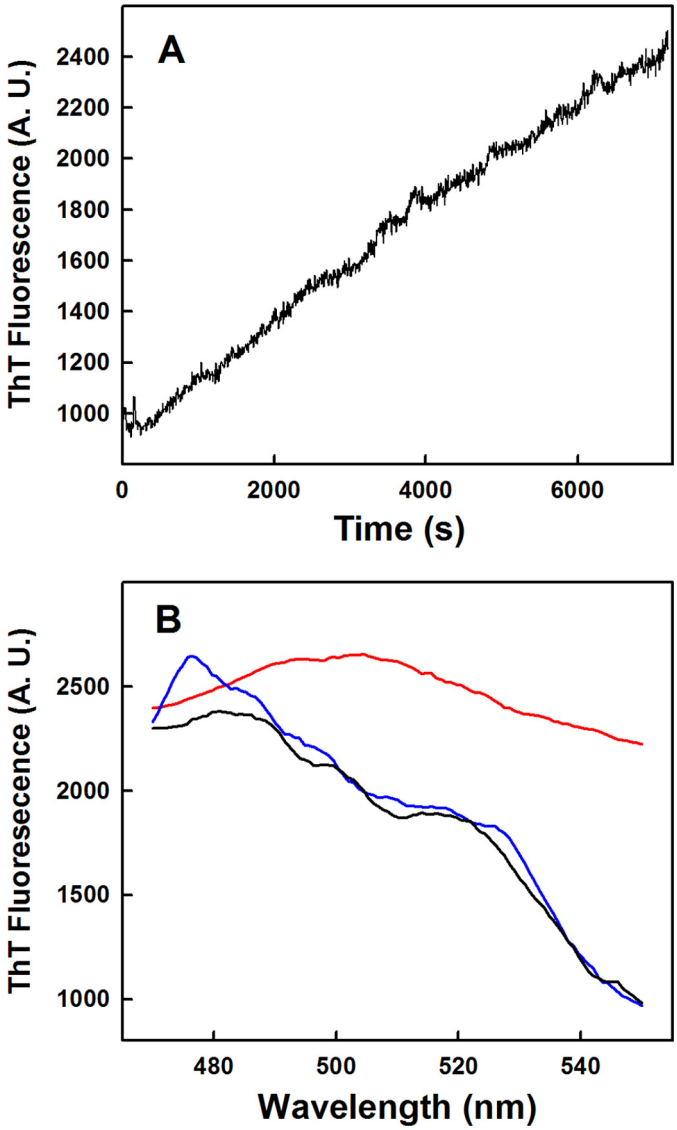

FIGURE 3. **Full-length p53 aggregation followed by an increase in ThT fluorescence.** *A*, 2-h kinetics of p53 aggregation followed by ThT binding and an increase in ThT fluorescence. Excitation: 450 nm, emission: 510 nm. *B*, ThT spectra in the absence (*black line*) and presence of p53. The *blue line* corresponds to soluble p53, and the *red line* corresponds to the ThT spectrum after 12 h of p53 aggregation.

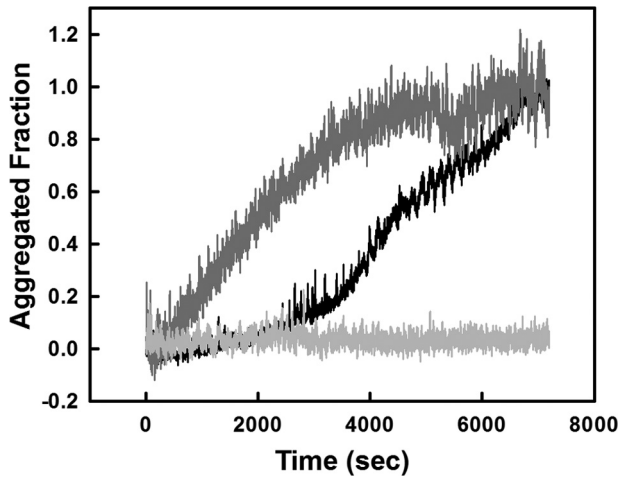

FIGURE 4. **Seeding of wild-type p53 aggregation by aggregated R248Q.** Aggregation was monitored by thioflavin T fluorescence emission (excitation: 450 nm; emission: 482 nm) over time at 37 °C. Wild-type p53 at 10 μM (*black line*) or R248Q at 20 μM was incubated at 37 °C for 30 min, and after 10-fold dilution, the protein was added to 10 μM wild-type p53 (*dark gray line*). Also, R248Q was seeded alone at 2 μM as a control (*gray line*). The concentration of ThT was 35 μM, and measurements were performed at pH 7.2 in 10 mM Tris buffer, 150 mM NaCl, 5% glycerol, and 5 mM DTT. The aggregated fraction = $(F_{obs} - F_I)/(F_F - F_I)$, where F is the ThT fluorescence emission intensity, F_{obs} represents the observed fluorescence emission, F_I is the initial fluorescence, and F_F is the final fluorescence.

meric species isolated at pH 7.2 were more heterogeneous than those obtained at pH 5.0, yielding Rh values between 80 and 125 nm for both WT and R248Q p53C at 7.2. It is interesting to note that, for both mutant and wild-type p53C, the aggregates formed at pH 7.2 presented a higher Rh than those formed at pH 5.0.

To evaluate whether the aggregation properties found for p53C and other domains were present in the full-length protein, we examined the aggregation at physiological conditions. Even at relatively low protein concentrations, full-length p53 underwent aggregation at 37 °C with kinetics very similar to those of p53C (Fig. 3*A*). Moreover, the ThT spectrum collected after 12 h was typical of those of amyloid-bound dyes (Fig. 3*B*).

Seeding of Wild-type p53 Aggregation by R248Q Mutant Oligomers and Fibrils—One important question that emerged was whether the higher aggregation propensity of the R248Q mutant was related to the negative dominance effect observed *in vivo*. To verify the molecular mechanism of this conversion, we performed a classical seeding experiment (Fig. 4). R248Q was aggregated by incubation at 37 °C for 30 min and, after performing a 10-fold dilution, it was added to wild-type p53. There was a clear suppression of the lag phase of wild-type p53 aggregation (*dark gray line*), demonstrating the significant seeding potential of the aggregated mutant protein.

Structural Characterization of the Aggregates—The aggregates of p53C were characterized structurally and functionally using x-ray diffraction, A11 antibody binding and cytotoxicity assays. The amyloid nature of p53 aggregates remains controversial. To further evaluate the aggregation of p53C, we followed ThT fluorescence during the pressurization and heat treatment of soluble p53C and observed that p53C aggregation in samples incubated at pH 7.2 was much greater than that in samples incubated at pH 5.0 (Fig. 5, *A* and *B*). The R248Q aggregate bound more ThT than WT p53C at a high temperature and pH 7.2 (Fig. 5*B*), whereas the opposite was observed for the HP treatment at pH 7.2, where WT p53C bound more ThT than did R248Q (Fig. 5*A*). Both protein constructs showed similar ThT binding at pH 5.0, regardless of the treatment (HP or HT) used (Fig. 5, *A* and *B*).

It is known that both fibrillar and ordered aggregates have additional β-sheet secondary structure than the native protein (11). Therefore, we used circular dichroism (CD) to evaluate the secondary structure content of mutant p53C (R248Q) upon incubation at pH 7.2 and 5.0 (Fig. 5*C*) in its soluble and aggregated states. All spectra showed a β-sheet-rich profile, as previously demonstrated for both soluble and aggregated wild-type proteins (3, 27). Note that the CD spectra of both HT aggregates (Fig. 5*C* and supplemental Fig. S1*A*) at pH 5.0 demonstrated greater β-sheet content than the soluble samples.

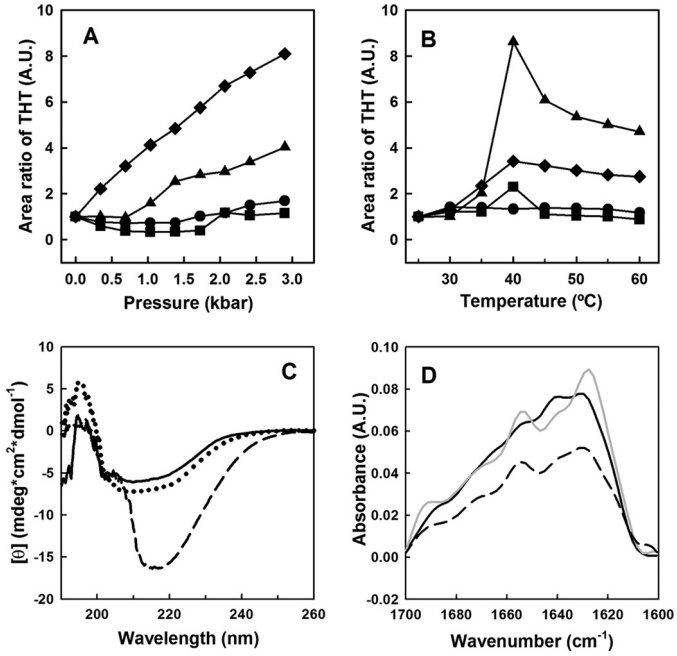

FIGURE 5. **Characterization of WT p53C and R248Q aggregation induced by high pressure, high temperature, or incubation at 37 °C for 2 h.** *A*, WT p53C at pH 7.2 (*diamond*) or pH 5.0 (*circle*) and R248Q at pH 7.2 (*triangle*) or pH 5.0 (*square*) at 5 μM were subjected to increasing pressures (up to 3 kbar) or to (*B*) temperatures ranging from 25 °C to 60 °C, and aggregation was monitored according to ThT fluorescence (50 μM). *C*, Far-UV CD spectra of R248Q p53C at pH 7.2 (*solid line*), pH 5.0 (*dotted line*) and after HT-induced aggregation at pH 5.0 (*dashed line*). ThT was excited at 450 nm, and light emission was collected from 470 to 530 nm. *D*, FTIR spectra of non-aggregated R248Q p53C (*solid line*) and 37T-aggregate of R248Q p53C obtained at pH 7.2 (*dashed line*) or at pH 5.0 (*gray*).

We also analyzed the secondary structural content of soluble and aggregated forms of p53C by FTIR. After aggregation, the samples were dialyzed against water and further lyophilized and deposited directly onto the ATR surface. The amide I region (1700 to 1600 cm^{-1}) was deconvoluted, and the secondary structure components were assigned as previously described (17, 18). Although the secondary structure differences were not great, we observed increased β-sheet content in the aggregates of both WT p53C and mutant R248Q (supplemental Table S1; Fig. 5*D*; supplemental Fig. S1, *B* and *C*). The FTIR results demonstrated more extensive β-sheet content at pH 5.0 than at pH 7.2, which corroborates the circular dichroism data (Fig. 5*C* and supplemental Table S1). The integral intensities of each identified secondary structure component after deconvolution and curve fitting of the amide I region are shown in supplemental Table S1.

The p53C Aggregates Interact with Anti-amyloid Oligomers—Conformation-dependent antibodies are powerful tools for examining misfolding and the mechanisms of amyloid formation. The A11 antibody binds to an epitope that is common to several types of amyloid oligomers and is unable to recognize the native protein (19). We evaluated A11-binding by p53C under various conditions by dot-blot assay and observed that only the samples at pH 7.2 were strongly labeled by the antibody (Fig. 6*A*). One potential explanation for this finding is that only p53C aggregates formed at pH 7.2 have the typical aggregation properties of amyloid oligomers and fibrils.

p53C Aggregates Exhibit an Amyloid-like Pattern—The x-ray diffraction pattern of the HP aggregate of WTp53C and R248Q at pH 7.2 was consistent with the typical conformation of cross β-sheet amyloid fibers with 4.7 Å and 10 Å reflections (7, 28) (Fig. 6, *B* and *C*). Although the HP aggregate at pH 5.0 also formed fibers, as observed by TEM (Fig. 6*D*), we were unable to collect x-ray diffraction data for this sample. For the HT aggregate, we observed typical amyloid diffractions of WT p53C at pH 7.2 and pH 5.0 and of R248Q at pH 7.2 (supplemental Fig. S2). As the x-ray diffraction pattern exhibits an amyloid fibril "fingerprint", these findings indicate that p53C forms fibrillar aggregates under the conditions described above. TEM was used to characterize the morphology of the p53C HT and HP aggregates. We aimed to correlate the different types of aggregates obtained with the physical treatments used, *i.e.* high pressure and high temperature at either pH 7.2 or 5.0. The TEM images were obtained at room temperature immediately after the treatments were carried out (Fig. 6*D*), and we observed that the p53C aggregates were mostly fibrillar, although non-fibrillar aggregates were also visualized. Different populations of amyloid oligomers could also be observed; these aggregates represent typical precursors of fibrils and include annular (doughnut-shaped) species. Moreover, the R248Q aggregates had a morphology similar to that of the wild-type aggregates.

The heterogeneity of the p53C aggregates was also evident from the analysis of Congo red birefringence (Fig. 2, *B* and *C*). For all the conditions used to produce aggregates, we found areas with apple-green birefringence under polarized light, typical of amyloid fibrils (Fig. 2). There were also areas with anomalous colors, which have been also assigned to amyloid aggregates (21).

p53C Aggregates Are Toxic to Cells in Culture—Cell viability assays after exposure to amyloid aggregates have been used for several proteins involved in human diseases (11, 26, 29–31). To determine whether the aggregates of p53C would be cytotoxic, as other amyloidogenic proteins, we performed a cell viability assay (LIVE/DEAD). Vero cells were exposed to HP or HT aggregates of WT p53C or R248Q obtained at pH 7.2 or 5.0 for 48 h (Fig. 7). We observed a co-localization of dead cells and the deposition of aggregates (Fig. 7*B*), whereas exposure to soluble wild-type and R248Q p53C was much less cytotoxic (Fig. 7*A*). In addition, there was no distinction between the cytotoxicity of wild-type and mutant protein aggregates. Cytoxicity is not a property of p53 aggregates only, but allowed us to reveal common characteristics between p53C aggregates and those formed by proteins involved in amyloid diseases. The fluorescence intensities could not be compared between live and dead cells because the p53C aggregates also reacted with calcein, our marker for live cells.

Wild-type p53 and Mutant R248Q Aggregates in Tumor Biopsies—We next analyzed whether p53 aggregation takes place in diseased tissues, particularly aggregates of R248Q, which demonstrated a greater tendency to aggregate *in vitro*. We detected p53 aggregates using an immunofluorescence co-localization assay with A11 and anti-p53 DO1 antibodies for archived samples of breast cancer tissues expressing mutant R248Q and wild-type p53, as previously described (9). Intense antibody binding was observed in p53 mutant cancer cells with

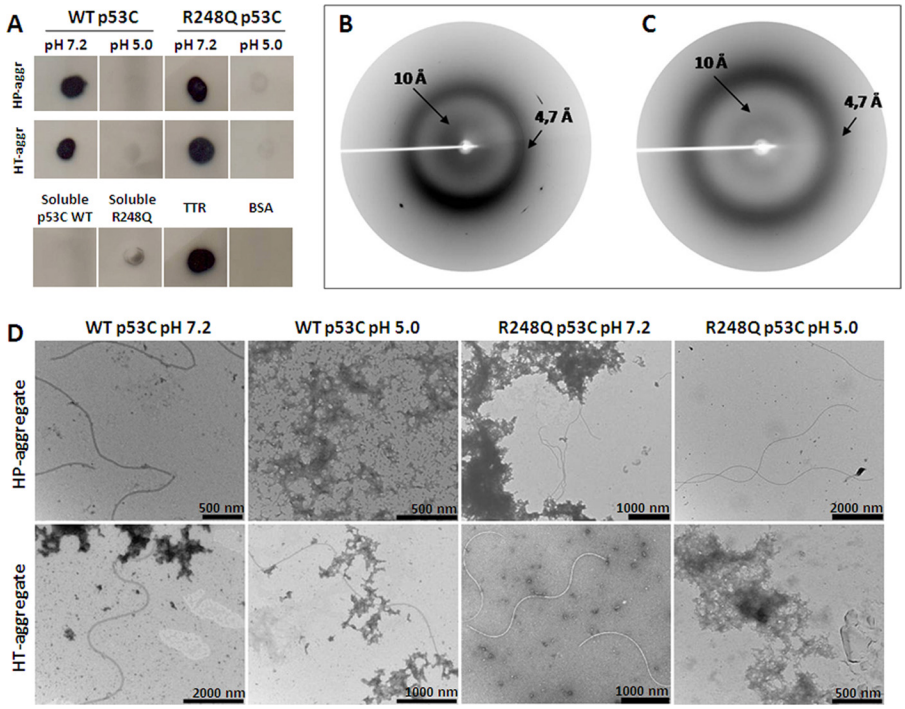

FIGURE 6. **p53C amyloid aggregates characterized by dot-blot immunoassay (*A*), x-ray diffraction (*B* and *C*), and TEM (*D*).** *A*, HP aggregate, HT aggregate, or WT p53C at pH 7.2, WT p53C at pH 5.0, R248Q at pH 7.2, R248Q at pH 5.0, soluble WT p53C, soluble R248Q, aggregated TTR, and soluble BSA. X-ray diffraction spectra of (*B*) p53C WT and (*C*) the R248Q HP-aggregate at pH 7.2. *D*, TEM analysis of the HT and HP aggregates of WT p53C and R248Q at pH 7.2 and pH 5.0. Samples at 5 μM were subjected to increasing temperatures up to 60 °C and pressures up to 3 kbar at 37 °C, and TEM images were collected immediately after the treatments.

anti-p53 and anti-oligomer A11, demonstrating a strong co-localization signal (Fig. 8).

The R248Q breast tissue biopsy was obtained from a patient with invasive ductal carcinoma of Elston grade 3. The tumor was negative for estrogen and progesterone receptors. Previously, we found that other hot-spot mutations demonstrated a high co-localization of p53 in amyloid-like aggregates (9).

Conversely, in wild-type cancer cells, we detected few cells with clear co-localization spots in only one of four samples (Fig. 8). It is possible that p53 was inactive in these samples or in some alternative conformation that would promote the formation of aggregates.

Co-localization of Full-length p53 and Aggregates in Tumor Cell Lines—To analyze the p53 aggregation pattern in breast cancer cell lines, we performed immunofluorescence co-localization experiments by labeling endogenous p53 and aggregates in MCF-7 cells, which express wild-type p53, and in MDA-MB 231 cells, which express the R280K p53 mutant. Confocal microscopy images revealed a weak distribution of wild-type p53 in the cytosol and punctate labeling near the perinuclear region (*arrowheads*, Fig. 9) in MCF-7 cells. However, predominant nuclear localization of mutated-p53 was observed in MDA-MB 231 cells. In these cells, mutated p53 strongly co-localized with the aggregates and was totally entrapped in the nuclear region (N) (Fig. 9*A*).

To further confirm that the aggregates contained p53, we performed SEC of the proteins extracted from the MCF-7 and MDA-MB 231 tumoral cell lines followed by p53 Western-blotting detection (Fig. 9, *B* and *C*). p53 aggregates were eluted in the void volume of the column, and a greater amount of p53 was eluted as aggregates, other than as tetramers in the tumoral cell lines.

DISCUSSION

In this report, we described p53 aggregation into amyloid structures at pH values of 7.2 and 5.0, which occur naturally in the cellular environment. In addition, we show for the first time that full-length p53 is prone to aggregate at 37 °C under physiological conditions. Remarkably, R248Q amyloid oligomers and fibrils were able to seed the aggregation of WT p53, which is a behavior typical of prions. We also detected p53 aggregates in breast cancer biopsy samples expressing the somatic mutation R248Q and in the nuclei of tumoral cells expressing the R280K mutation. Our study also provides the first description of the p53 core domain amyloid pattern based on x-ray diffraction and labeling with anti-oligomer A11 antibody under mild conditions. Moreover, the heterogeneous character of p53 aggregation was shown by transmission electron microscopy. Each of these approaches provided valuable information regarding the nature of the p53 fibrils and amyloid oligomers.

The accumulation of p53 is related to a loss-of-function of this protein and has been observed in various cancers including neuroblastoma, retinoblastoma, breast and colon cancers (22, 32, 33). A better understanding of how aggregates form and their nature is crucial to fully dissect this mechanism, which is potentially related to cancer.

We performed three procedures to obtain p53 aggregates. In all cases, we found that p53C aggregation was greater at pH 7.2 than at pH 5.0 (Figs. 1*A* and 5). TEM analysis showed that the 37T, HT, and HP aggregates formed fibrillar and amorphous

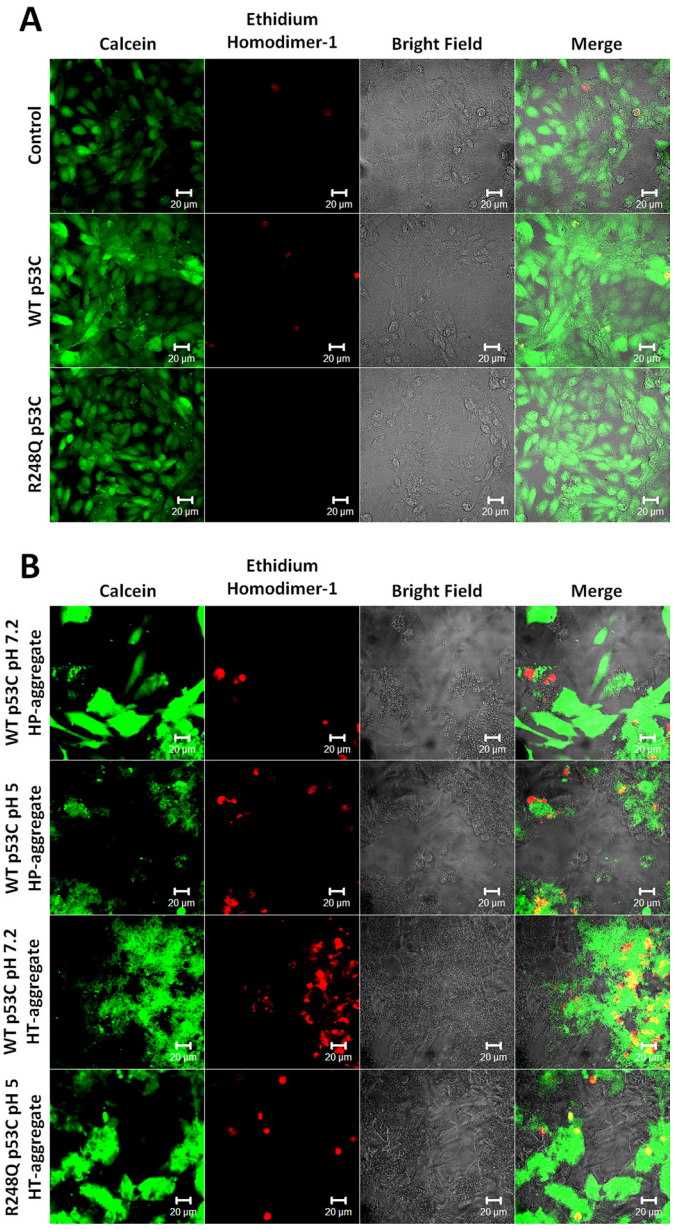

FIGURE 7. **Cytotoxicity evaluation of HP and HT aggregates of WT and R248Q p53C.** Soluble p53C (*A*) and aggregated p53C (*B*) at 4 μM were added to Vero cells, and cell viability was measured using a LIVE/DEAD assay 48 h later. The *first panel* represents a control consisting of exposure to buffer only.

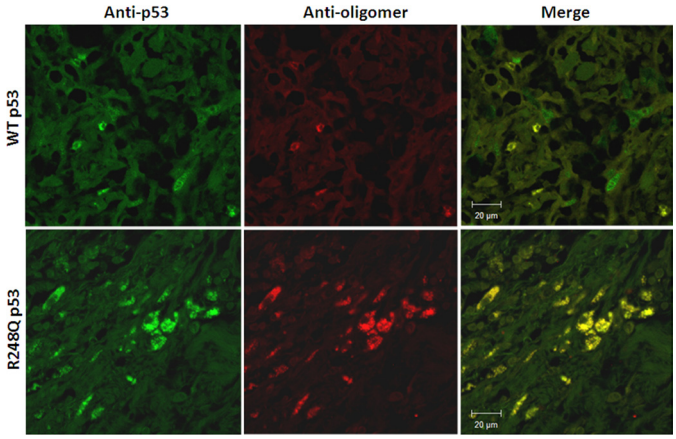

FIGURE 8. **Detection of native and aggregated p53 in tumor biopsy samples.** Paraffin-embedded breast cancer tissues expressing WT p53 or R248Q. The samples were labeled with anti-p53 DO1 and anti-oligomer A11 antibodies. The first column shows p53-labeling, the second column shows the labeling of aggregates, and the third column shows the merged images of p53-labeling and A11-labeling. The images were obtained at 40,000× magnification.

aggregates at both pH values evaluated (Figs. 1*B* and 5*D*). Moreover, the CD and FTIR data demonstrate that the aggregate forms of WT and mutant p53C possess more β-sheet content than the soluble species, and significantly bind to Congo Red (Figs. 2 and 5, *C* and *D*), which is typical of amyloid fibril formation (9).

The x-ray diffraction data exhibited an amyloid pattern for both WT p53C and R248Q samples subjected to high pressure and high temperature (Fig. 6, *B* and *C* and supplemental Fig. S2). These diffraction patterns revealed characteristic amyloid reflections (4.7 Å and 10 Å) due to the spacing in the regular repetitions of cross-β structures (28). Another region of p53 has also been described to aggregate into amyloid structures when incubated at pH 3.0 (7).

Oligomers, which occur within the pathway to fibril formation, have been described as the toxic species in amyloid diseases (34, 35). To evaluate the amyloid oligomers of p53C, we used the anti-oligomer antibody A11 (19) and found that only the HT and HP aggregates were labeled by the antibody at pH 7.2 (Fig. 6*A*). It is possible that only the aggregates that formed at pH 7.2 contained a significant population of amyloid oligomeric precursors following the period chosen for incubation.

Moreover, we found that p53C aggregates induced cell death, as other amyloidogenic proteins. Cell death occurred in the presence of fibrillar or amyloid oligomers (WT and R248Q mutant p53) (Fig. 7). Previous studies using an MTT reduction assay indicated that aggregates of WT p53C (obtained at pH 7.2) could cause cellular dysfunction in cultured macrophages (3). N-terminal aggregates of p53 have also been shown to be cytotoxic (7). This behavior of p53 aggregates is also similar to that observed for aggregates of mammalian prion proteins (14, 26).

Mutant p53 proteins often accumulate at extremely high levels in tumors (36). In fact, immunohistochemical analyses of p53 in tumors have detected mutant p53 produced by gene missense mutations, which are related to poor cancer prognoses (37). In addition, in a subset of tumors, inactive wild-type p53 is retained in the cytoplasm and impairs the transcription factor activity of the active p53 species (22, 32, 33).

To determine whether full-length p53 would also undergo aggregation, we evaluated the p53 status in diseased tissues. Aggregates of p53 were detected in breast cancer tissue samples using an immunofluorescence co-localization assay (Fig. 8). Most interestingly, we identified the mutant R248Q protein in the amyloid-like aggregated state in a breast cancer sample expressing this hot-spot mutant (Fig. 8). In our previous work (9), we demonstrated that the R273H mutant had a high propensity to form amyloid-like aggregates, whereas the hot-spot mutant R175H co-localized with amyloid-like species in very few cells. These observations suggest that p53 aggregation may be dependent on mutation type. Our *in vitro* and *ex vivo* results

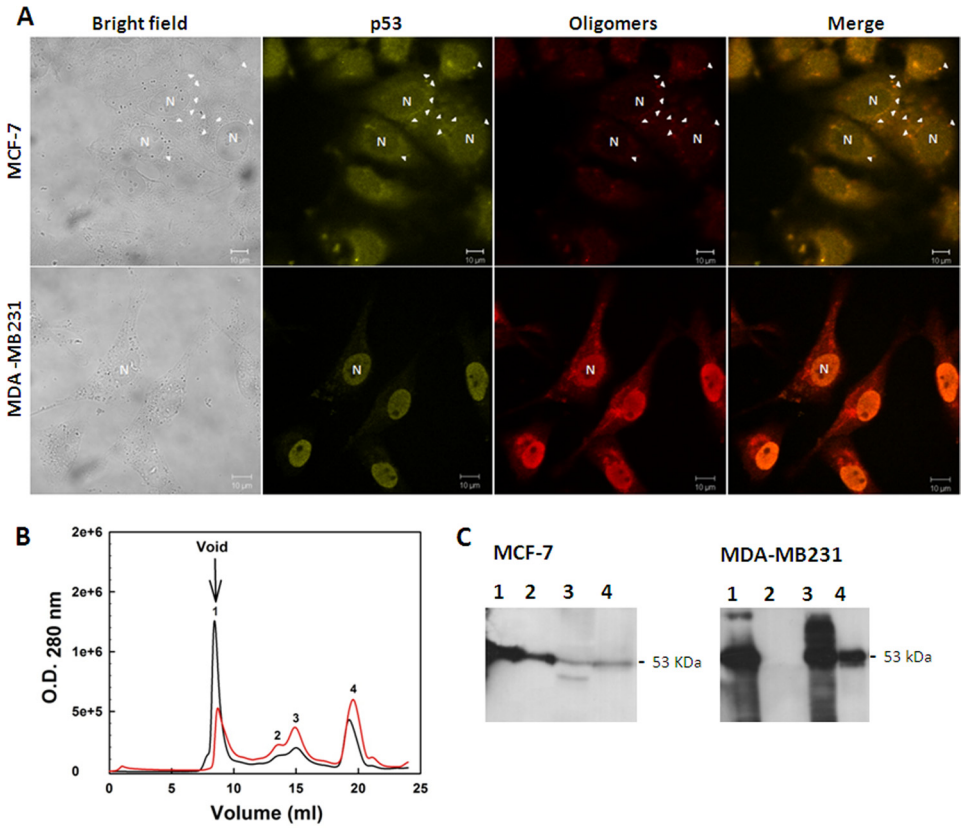

FIGURE 9. **Detection of native and aggregated p53 in breast cancer cell lines.** *A*, MCF-7 (wild-type p53) and MDA-MB 231 (mutated p53) cells were labeled with anti-p53 (DO-1) and anti-oligomer (A11) primary antibodies. The *first column* shows the bright field images, the *second column* shows p53-labeling, the *third column* shows the labeling of aggregates, and the *last column* shows the merged images of p53 labeling and aggregate labeling. The images were obtained at 63,000× magnification. *B*, size exclusion chromatography fractions (SEC) of the extract of the MCF-7 (*red line*) and MDA-MB 231 (*black line*) tumoral cell lines. Western blotting against p53 was carried out for the eluted fractions (*C*). Aggregated p53 eluted in the column void volume.

suggest that the mutant R248Q is prone to aggregate in tumors. Moreover, the high degree of co-localization between p53 and the aggregates also indicates that *in vivo* cells expressing the mutant isoform lead to the co-aggregation of the wild-type isoform, which further supports the evidence for the prion-like action of these proteins.

The significantly higher aggregation propensity of mutant p53 was confirmed by the co-localization of full-length p53 and aggregates in tumoral cell lines (Fig. 9). Whereas there was a very faint labeling of p53 aggregates in the wild-type p53 cell line (MCF-7), there was significant labeling in the nuclei of aggregates of mutant p53 in MDA-MB 231 cells.

Our results strongly suggest a correlation between p53 mutation and p53 aggregation in cells. We propose that the buildup and further aggregation of mutants into ordered species is caused by an inhibition of the degradation process, which may be due to defects in MDM2 protein expression or p53 ubiquitination (37–39), as both processes are known to be involved in p53 clearance. In addition, altered cellular trafficking of p53 could lead to abnormal accumulation of p53 in the nucleus or cytoplasm, which would prevent the protein from exerting its normal functions (for a review, see Refs. 36 and 40). This seemed to be the case for the results obtained with tumoral cell lines harboring the R280K mutant of p53, where massive p53 aggregation in the nuclei was found (Fig. 9).

It has been suggested that higher concentrations of p53 mutants promote a negative dominance mechanism (41). According to one hypothesis, wild-type p53 molecules, which are present at a lower concentration, may form heterotetramers with mutants to result in a reduced p53 affinity for DNA (42). Our group has previously proposed an alternative hypothesis for the negative dominance effect, in which wild-type p53 at lower concentrations would be incorporated into aggregates containing the mutant species (3, 4).

The presence of a misfolded conformation would sequester the correctly folded form, thus suppressing function. This view is consistent with a prion-like mechanism, where the pathogenic species acts as an altered molecular chaperone to induce the correctly folded native protein to acquire the misfolded conformation, thereby increasing aggregation. In the case of p53, mutant forms may be even more susceptible to aggregation, which would amplify this process (Fig. 10). Finally, we propose that aggregation of p53 may act as a sink to sequestrate the native protein into the inactive conformation via a mechanism typical of a prionoid (43, 44).

The observation that WT and mutant p53 forms aggregate as amyloids, which are associated with the negative dominant effect, adds an amyloid characteristic to cancer. In a recent review article, Antony *et al.* (14) discussed the potential role of prions and protein-only inheritance in cancer. They argue how

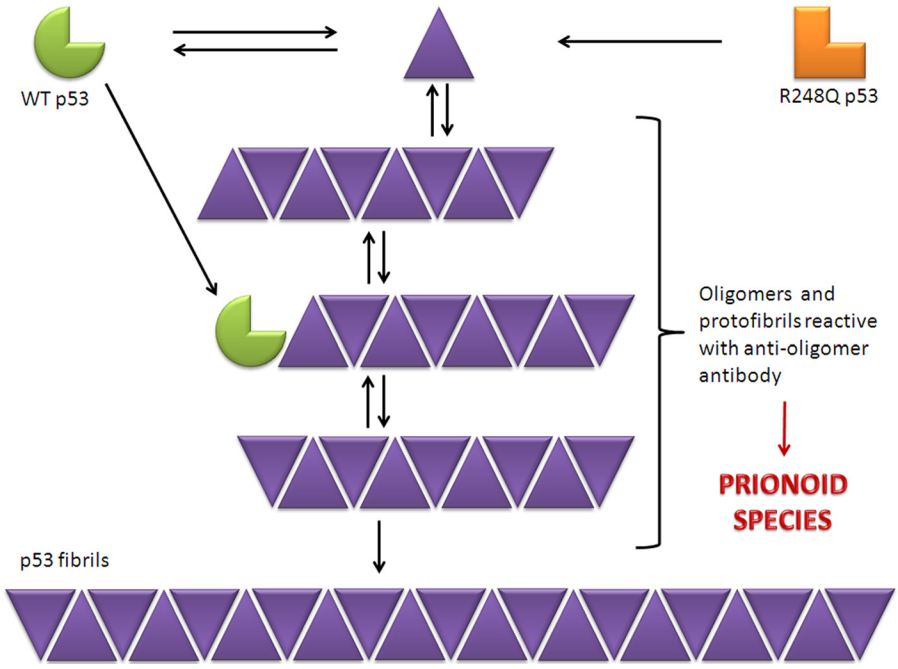

FIGURE 10. **Schematic model for the prionoid conversion and negative dominance of mutant p53.** The native conformations of WT and R248Q p53 are represented as *green* and *orange* molecules, respectively. The misfolded conformation of either molecule is represented in *purple*. According to the model, the prion-like character responsible for the negative dominance effect would occur in the oligomers.

somatic inheritance in mammalian cells (including p53) may contribute to cancer phenotypes, and these authors also stress how the involvement of prion-like mechanisms in cancer can lead to novel therapeutic targets.

Fig. 10 presents a schematic diagram for how misfolded p53 could divert native protein into aggregates and how the mutant form, with its greater propensity for aggregation, would lead to a negative dominance effect. This diagram has evolved from a previous proposal (3) by incorporating the results demonstrating the seeding potential of R248Q aggregates and our findings that both wild-type and mutant p53 form heterogeneous mixtures of amyloid oligomers and amyloid fibrils. Hetero-oligomerization is more likely to occur in smaller aggregates, and the formation of fibrils leads the system toward fewer reversible species. Thus, in contrast to previous proposals (3, 10), the heterogeneous character of the amyloid aggregates is the key feature that leads to the negative dominance effect, not only the tendency to form fibrils. This feature also likely explains why the anti-oligomer antibody bound a significant amount of targets in tumor tissues containing the R248Q mutation.

At low pH, there was less formation of fibrillar p53 species. Aggregation at acidic pH may occur in some cellular compartments, such as lysosomes, endosomes, and proteasomes, which are associated with protein translocation and degradation. It has been reported that p53 adopts a molten-globule state at low pH (24) and would therefore have a lower tendency toward aggregation. It is noteworthy that the molten-globule state of the p53 DNA-binding domain is the client conformation for interaction with the chaperone Hsp90 (45).

The prionoid character of mutant p53 is also a potential target for therapeutic action. Aptameric nucleic acids and glycosaminoglycans have been evaluated as drug candidates against mammalian prions (46–48) and therefore represent strong candidates to tackle p53 prion-like aggregation. Moreover, complementary studies may reveal the biological and clinical importance of p53 aggregates and help to develop new strategies for intervening against aggregation formation.

Acknowledgments—We thank Martha M. Sorenson for carefully reading the manuscript and providing helpful suggestions. We also thank Mariana P. B. Gomes for suggestions and aid in the drawing of Fig. 10.

REFERENCES

1. Vousden, K. H., and Lane, D. P. (2007) p53 in health and disease. *Nat. Rev. Mol. Cell Biol.* **8,** 275–283
2. Joerger, A. C., and Fersht, A. R. (2008) Structural biology of the tumor suppressor p53. *Annu. Rev. Biochem.* **77,** 557–582
3. Ishimaru, D., Andrade, L. R., Teixeira, L. S., Quesado, P. A., Maiolino, L. M., Lopez, P. M., Cordeiro, Y., Costa, L. T., Heckl, W. M., Weissmüller, G., Foguel, D., and Silva, J. L. (2003) Fibrillar aggregates of the tumor suppressor p53 core domain. *Biochemistry* **42,** 9022–9027
4. Silva, J. L., Vieira, T. C., Gomes, M. P., Ano Bom, A. P., Lima, L. M., Freitas, M. S., Ishimaru, D., Cordeiro, Y., and Foguel, D. (2010) Ligand binding and hydration in protein misfolding: insights from studies of prion and p53 tumor suppressor proteins. *Acc. Chem. Res.* **43,** 271–279
5. Galea, C., Bowman, P., and Kriwacki, R. W. (2005) Disruption of an intermonomer salt bridge in the p53 tetramerization domain results in an increased propensity to form amyloid fibrils. *Prot. Sci.* **14,** 2993–3003
6. Higashimoto, Y., Asanomi, Y., Takakusagi, S., Lewis, M. S., Uosaki, K., Durell, S. R., Anderson, C. W., Appella, E., and Sakaguchi, K. (2006) Unfolding, aggregation, and amyloid formation by the tetramerization domain from mutant p53 associated with lung cancer. *Biochemistry* **45,** 1608–1619
7. Rigacci, S., Bucciantini, M., Relini, A., Pesce, A., Gliozzi, A., Berti, A., and Stefani, M. (2008) The (1–63) region of the p53 transactivation domain aggregates *in vitro* into cytotoxic amyloid assemblies. *Biophys. J.* **94,**

3635–3646
8. Ishimaru, D., Ano Bom, A. P., Lima, L. M., Quesado, P. A., Oyama, M. F., de Moura Gallo, C. V., Cordeiro, Y., and Silva, J. L. (2009) Cognate DNA stabilizes the tumor suppressor p53 and prevents misfolding and aggregation. *Biochemistry* **48,** 6126–6135
9. Levy, C. B., Stumbo, A. C., Ano Bom, A. P., Portari, E. A., Cordeiro, Y., Silva, J. L., De Moura-Gallo, C. V. (2011) Co-localization of mutant p53 and amyloid-like protein aggregates in breast tumors. *Int. J. Biochem. Cell Biol.* **43,** 60–64
10. Xu, J., Reumers, J., Couceiro, J. R., De Smet, F., Gallardo, R., Rudyak, S., Cornelis, A., Rozenski, J., Zwolinska, A., Marine, J. C., Lambrechts, D., Suh, Y. A., Rousseau, F., and Schymkowitz, J. (2011) Gain of function of mutant p53 by coaggregation with multiple tumor suppressors. *Nat. Chem. Biol.* **7,** 285–295
11. Chiti, F., and Dobson, C. M. (2006) Protein misfolding, functional amyloid, and human disease. *Annu. Rev. Biochem.* **75,** 333–366
12. Pastore, A., and Temussi, P. A. (2012) The two faces of Janus: functional interactions and protein aggregation. *Curr. Opin. Struct. Biol.* **22,** 30–37
13. Butler, J. S., and Loh, S. N. (2003) Structure, function, and aggregation of the zinc-free form of the p53 DNA binding domain. *Biochemistry* **42,** 2396–2403
14. Antony, H, Wiegmans, A. P., Wei, M. Q., Chernoff, Y. O., Khanna, K. K., and Munn, A. L. (2011) Potential roles for prions and protein-only inheritance in cancer. *Cancer Metastasis Rev.* **31,** 1–19
15. Hollstein, M., Sidransky, D., Vogelstein, B., and Harris, C. C. (1991) p53 mutations in human cancers. *Science* **253,** 49–53
16. Olivier, M., Hollstein, M., and Hainaut, P. (2010) TP53 mutations in human cancers: origins, consequences, and clinical use. *Cold Spring Harb. Perspect. Biol.* **2,** a001008
17. Cordeiro, Y., Kraineva, J., Gomes, M. P., Lopes, M. H., Martins, V. R., Lima, L. M., Foguel, D., Winter, R., and Silva, J. L. (2005) The amino-terminal PrP domain is crucial to modulate prion misfolding and aggregation. *Biophys. J.* **89,** 2667–2676
18. Cordeiro, Y., Kraineva, J., Ravindra, R., Lima, L. M., Gomes, M. P., Foguel, D., Winter, R., and Silva, J. L. (2004) Hydration and packing effects on prion folding and β-sheet conversion. High pressure spectroscopy and pressure perturbation calorimetry studies. *J. Biol. Chem.* **279,** 32354–33259
19. Glabe, C. G. (2004) Conformation-dependent antibodies target diseases of protein misfolding. *Trends Biochem. Sci.* **29,** 542–547
20. Lai, Z., Colón, W., and Kelly, J. W. (1996) The acid-mediated denaturation pathway of transthyretin yields a conformational intermediate that can self-assemble into amyloid. *Biochemistry* **35,** 6470–6482
21. Howie, A. J., Brewer, D. B., Howell, D., and Jones, A. P. (2008) Physical basis of colors seen in Congo red-stained amyloid in polarized light. *Lab. Invest.* **88,** 232–242
22. Moll, U. M., LaQuaglia, M., Bénard, J., and Riou, G. (1995) Wild-type p53 protein undergoes cytoplasmic sequestration in undifferentiated neuroblastomas but not in differentiated tumors. *Proc. Natl. Acad. Sci. U.S.A.* **92,** 4407–4411
23. Ostermeyer, A. G., Runko, E., Winkfield, B., Ahn, B., and Moll, U. M. (1996) Cytoplasmically sequestered wild-type p53 protein in neuroblastoma is relocated to the nucleus by a C-terminal peptide. *Proc. Natl. Acad. Sci. U.S.A.* **93,** 15190–15194
24. Bom, A. P., Freitas, M. S., Moreira, F. S., Ferraz, D., Sanches, D., Gomes, A. M., Valente, A. P., Cordeiro, Y., and Silva, J. L. (2010) The p53 core domain is a molten globule at low pH: functional implications of a partially unfolded structure. *J. Biol. Chem.* **285,** 2857–2866
25. Gerweck, L. E. (1998) Tumor pH: implications for treatment and novel drug design. *Semin. Radiat. Oncol.* **8,** 176–182
26. Gomes, M. P., Millen, T. A., Ferreira, P. S., e Silva, N. L., Vieira, T. C., Almeida, M. S., Silva, J. L., and Cordeiro, Y. (2008) Prion protein complexed to N2a cellular RNAs through its N-terminal domain forms aggregates and is toxic to murine neuroblastoma cells. *J. Biol. Chem.* **283,** 19616–19625
27. Ishimaru, D., Lima, L. M., Maia, L. F., Lopez, P. M., Ano Bom, A. P., Valente, A. P., and Silva, J. L. (2004) Reversible aggregation plays a crucial role on the folding landscape of p53 core domain. *Biophys. J.* **87,** 2691–2700
28. Sunde, M., Serpell, L. C., Bartlam, M., Fraser, P. E., Pepys, M. B., and Blake, C. C. (1997) Common core structure of amyloid fibrils by synchrotron X-ray diffraction. *J. Mol. Biol.* **273,** 729–739
29. Novitskaya, V., Bocharova, O. V., Bronstein, I., and Baskakov, I. V. (2006) Amyloid fibrils of mammalian prion protein are highly toxic to cultured cells and primary neurons. *J. Biol. Chem.* **281,** 13828–13836
30. Vieira, M. N., Forny-Germano, L., Saraiva, L. M., Sebollela, A., Martinez, A. M., Houzel, J. C., De Felice, F. G., and Ferreira, S. T. (2007) Soluble oligomers from a non-disease related protein mimic Aβ-induced tau hyperphosphorylation and neurodegeneration. *J. Neurochem.* **103,** 736–748
31. Gomes, M. P., Cordeiro, Y., and Silva, J. L. (2008) The peculiar interaction between mammalian prion protein and RNA. *Prion* **2,** 64–66
32. Elledge, R. M., Clark, G. M., Fuqua, S. A., Yu, Y. Y., and Allred, D. C. (1994) p53 protein accumulation detected by five different antibodies: relationship to prognosis and heat shock protein 70 in breast cancer. *Cancer Res.* **54,** 3752–3757
33. Moll, U. M., Valea, F., and Chumas, J. (1997) Role of p53 alteration in primary peritoneal carcinoma. *Int. J. Gynecol. Pathol.* **16,** 156–162
34. Lambert, M. P., Barlow, A. K., Chromy, B. A., Edwards, C., Freed, R., Liosatos, M., Morgan, T. E., Rozovsky, I., Trommer, B., Viola, K. L., Wals, P., Zhang, C., Finch, C. E., Krafft, G. A., and Klein, W. L. (1998) Diffusible, nonfibrillar ligands derived from Abeta1–42 are potent central nervous system neurotoxins. *Proc. Natl. Acad. Sci. U.S.A.* **95,** 6448–6453
35. Kayed, R., Head, E., Thompson, J. L., McIntire, T. M., Milton, S. C., Cotman, C. W., and Glabe, C. G. (2003) Common structure of soluble amyloid oligomers implies common mechanism of pathogenesis. *Science* **300,** 486–489
36. Gottifredi, V., and Prives, C. (2001) Molecular biology. Getting p53 out of the nucleus. *Science* **292,** 1851–1852
37. Soussi, T., and Béroud, C. (2001) Assessing TP53 status in human tumours to evaluate clinical outcome. *Nat. Rev. Cancer* **1,** 233–240
38. Chowdary, D. R., Dermody, J. J., Jha, K. K., and Ozer, H. L. (1994) Accumulation of p53 in a mutant cell line defective in the ubiquitin pathway. *Mol. Cell Biol.* **14,** 1997–2003
39. Chen, L., Lu, W., Agrawal, S., Zhou, W., and Zhang, R. (1999) Ubiquitous induction of p53 in tumor cells by antisense inhibition of MDM2 expression. *Mol. Med.* **5,** 21–34
40. Goh, A. M., Coffill, C. R., and Lane, D. P. (2011) The role of mutant p53 in human cancer. *J. Pathol.* **223,** 116–126
41. Joerger, A. C., Rajagopalan, S., Natan, E., Veprintsev, D. B., Robinson, C. V., and Fersht, A. R. (2009) Structural evolution of p53, p63, and p73: implication for heterotetramer formation. *Proc. Natl. Acad. Sci. U.S.A.* **106,** 17705–17710
42. Nicholls, C. D., McLure, K. G., Shields, M. A., and Lee, P. W. (2002) Biogenesis of p53 involves cotranslational dimerization of monomers and post-translational dimerization of dimers. Implications on the dominant negative effect. *J. Biol. Chem.* **277,** 12937–12945
43. Aguzzi, A., and Rajendran, L. (2009) The transcellular spread of cytosolic amyloids, prions, and prionoids. *Neuron* **64,** 783–790
44. Frost, B., and Diamond, M. I. (2010) Prion-like mechanisms in neurodegenerative diseases. *Nat. Rev. Neurosci.* **11,** 155–159
45. Park, S. J., Borin, B. N., Martinez-Yamout, M. A., and Dyson, H. J. (2011) The client protein p53 adopts a molten globule-like state in the presence of Hsp90. *Nat. Struct. Mol. Biol.* **18,** 537–541
46. Kocisko, D. A., Vaillant, A., Lee, K. S., Arnold, K. M., Bertholet, N., Race, R. E., Olsen, E. A., Juteau, J. M., and Caughey, B. (2006) Potent antiscrapie activities of degenerate phosphorothioate oligonucleotides. *Antimicrob. Agents Chemother.* **50,** 1034–1044
47. Caughey, B., Caughey, W. S., Kocisko, D. A., Lee, K. S., Silveira, J. R., and Morrey, J. D. (2006) Prions and transmissible spongiform encephalopathy (TSE) chemotherapeutics: A common mechanism for anti-TSE compounds? *Acc. Chem. Res.* **39,** 646–653
48. Vieira, T. C., Reynaldo, D. P., Gomes, M. P., Almeida, M. S., Cordeiro, Y., and Silva, J. L. (2010) Heparin binding by murine recombinant prion protein leads to transient aggregation and formation of RNA-resistant species. *J. Am. Chem. Soc.* **133,** 334–344